

# Femtoscopic study of the $S = -1$ meson-baryon interaction: $K^- p$ , $\pi^- \Lambda$ and $K^+ \Xi^-$ correlations

P. Encarnación,<sup>1,2,\*</sup> A. Feijoo,<sup>3,4,†</sup> V. Mantovani Sarti,<sup>3,‡</sup> and A. Ramos<sup>1,\*</sup>

<sup>1</sup>*Departament de Física Quàntica i Astrofísica and Institut de Ciències del Cosmos (ICCUB),  
Facultat de Física, Universitat de Barcelona, Barcelona, Spain*

<sup>2</sup>*Departamento de Física Teórica and IFIC, Centro Mixto Universidad de Valencia-CSIC,  
Institutos de Investigación de Paterna, Aptdo. 22085, E-46071 Valencia, Spain*

<sup>3</sup>*Physik Department E62, Technische Universität München, Garching, Germany, EU*

<sup>4</sup>*Instituto de Física Corpuscular, Centro Mixto Universidad de Valencia-CSIC,  
Institutos de Investigación de Paterna, Aptdo. 22085, E-46071 Valencia, Spain*

(Dated: December 31, 2024)

We study the femtoscopic correlation functions of meson-baryon pairs in the strangeness  $S = -1$  sector, employing unitarized s-wave scattering amplitudes derived from the chiral Lagrangian up to next-to-leading order. For the first time, we deliver predictions on the  $\pi^- \Lambda$  and  $K^+ \Xi^-$  correlation functions which are feasible to be measured at the Large Hadron Collider. We also demonstrate that the employed model is perfectly capable of reproducing the  $K^- p$  correlation function data measured by the same collaboration, without the need to modify the coupling strength to the  $\bar{K}^0 n$  channel, as has been recently suggested. In all cases, the effects of the source size on the correlation are tested. In addition, we present detailed analysis of the different coupled-channel contributions, together with the quantification of the relative relevance of the different terms in the interaction.

## I. INTRODUCTION

The scattering between kaons and nucleons has drawn the attention of the theoretical community in the last few decades [1–4]. The attractive character of the  $\bar{K}N$  interaction and the presence of a large number of resonant states around the  $\bar{K}N$  threshold offer a perfect testing ground for the chiral unitary approach. Indeed, the Unitarized Chiral Perturbation Theory framework (UChPT) has been shown to be a powerful tool to treat the low-energy meson-baryon interaction in the  $S = -1$  sector. The success of this non-perturbative scheme lies in the ability to reproduce the experimental data and the dynamic generation of bound states and resonances, as already proved in the early stages of this approach [5–13]. Among the generated states, the most outstanding one is the  $\Lambda(1405)$  resonance for its intricate nature, whose most plausible interpretation comes in terms of a double-pole contribution arising from coupled-channel meson-baryon re-scattering [8, 14, 15]. To illustrate the controversy around this state, it suffices to mention that although the dynamical origin of  $\Lambda(1405)$  was predicted in the late 1950s [16], this interpretation has found its way into the PDG compilation [17] only recently.

Continuing chronologically, one of the main messages appearing in Ref. [18] was the need for additional subthreshold information on the antikaon-nucleon dynamics to correctly locate the two poles associated to the  $\Lambda(1405)$  state. In order to amend the lack of constraints, the experimental machinery was set in motion, and several groups carried out new measurements that certainly shed some light on this topic. The  $\pi\Sigma$  mass distributions from  $pp$  scattering experiments were provided by the COSY and HADES collaborations, [19] and [20] respectively. Additional information came from JLAB, where

photo-production differential cross sections for the  $\Sigma(1385)$ ,  $\Lambda(1405)$ , and  $\Lambda(1520)$  in the reactions  $\gamma + p \rightarrow K^+ + Y^*$  were provided using the CLAS detector. Furthermore, the CLAS collaboration also reported on a direct determination of the expected spin-parity  $J^\pi = 1/2^-$  of the  $\Lambda(1405)$  [21]. However, the SIDDHARTA collaboration [22] performed the most striking measurement to constrain the theoretical models, which consists of the precise determination of the energy shift and width (around 20%) of the  $1s$  state in kaonic hydrogen. In this way, the tension between the DEAR [23, 24] and KEK [25] measurements, with almost a factor two of relative uncertainty, could be resolved. The availability of these experimental data again boosted the theoretical community [26–33], and the models were revisited, in some cases extended to higher orders and energies, with the aim of describing the observables within the new experimental uncertainties. It should be noted that, if the models are limited to accommodate the two-body cross sections of  $K^- p$  scattering into  $\pi\Sigma$ ,  $\bar{K}N$ ,  $\pi\Lambda$  states (the classical channels) or the experimental photo-production data on  $\gamma p \rightarrow K^+ \pi\Sigma$  reactions, the dominant contribution to reach a good agreement with the experimental data is the contact Weinberg-Tomozawa (WT) one. In other words, the incorporation of other ( $O(p)$ ) corrections, i. e. the direct and crossed Born terms, as well as the next-to-leading order (NLO) terms plays merely a fine-tuning role. In fact, the model in Ref. [29] was constrained by a larger set of data that included, apart from the classical cross sections and the scattering length extracted from the SIDDHARTA outputs, the scattering data from  $K^- p \rightarrow \eta\Lambda$ ,  $\pi^0\pi^0\Sigma^0$  and data from two event distributions ( $K^- p \rightarrow \Sigma^+(1660)\pi^- \rightarrow \Sigma^+\pi^-\pi^+\pi^-$  and  $K^- p \rightarrow \pi^0\pi^0\Sigma^0$ ). From there, one immediately realizes that the inclusion of NLO contribution improves remarkably the reproduction of the  $K^- p \rightarrow \eta\Lambda$  scattering data.

One of the challenges to be faced when incorporating the NLO terms of the chiral lagrangian is the determination of the corresponding low energy constants (LECs), which are not established by the underlying theory and should be ob-

\* ramos@fqa.ub.edu

† Corresponding author; albert.feijoo@tum.de

‡ valentina.mantovani-sarti@tum.de

tained through fitting procedures to experimental data sensitive to these higher order corrections. The  $K^-p \rightarrow K\Xi$  reactions are an example of such kind of processes, since they do not proceed via the WT term and the rescattering terms due to the coupled channels taken in the Bethe-Salpeter (BS) equation are not sufficient to reproduce the experimental cross section. In the series of papers [34, 35], the authors not only demonstrate the sensitivity of the  $K\Xi$  channels to the NLO terms but also obtained results that revealed the particular relevance of the u- and s-diagrams. A step further was given in [36], where, motivated by the findings of the former studies and aiming at more reliable values of the NLO coefficients, the  $K^-p \rightarrow \eta\Lambda, \eta\Sigma^0$  reactions were incorporated in the fits thereby having information from all possible channels of the  $S = -1$  sector. The model obtained (BCN model) is able to reproduce all the available low-energy scattering data from  $K^-p \rightarrow (S = -1)$  pseudoscalar-baryon processes with a very reasonable agreement, as well as all the  $\bar{K}N$  threshold observables typically employed in these studies (branching ratios and the scattering length extracted from the SIDDHARTA measurements [22]). The BCN model also does a good job in reproducing within errors the strength of the  $K^-n \rightarrow \pi^-\Lambda$  amplitude (30 MeV below  $\bar{K}N$  threshold), which was extrapolated from  $K^-$  absorption processes on  $^4\text{He}$  [37]. In the spirit of testing the validity of the BCN model at higher energies, a prediction of the  $K_L^0 p \rightarrow K^+\Xi^0$  cross section, proposed for its measurement at Jlab [38], was also given. Moreover, when implementing in-medium corrections including one- and two-nucleon absorption channels, the BCN model reproduces satisfactorily the antikaon absorption rates in  $^{12}\text{C}$  [39] and improves significantly the description of kaonic atom data [40].

Unfortunately, despite all previous experimental and theoretical advances, if one turns the attention to the amplitude behavior below the  $\bar{K}N$  threshold and compares what comes out employing different chirally motivated benchmark models, notable discrepancies can be appreciated. This is clearly illustrated in Fig. 1 of Ref. [41], which is particularized for  $K^-p$  and  $K^-n$  elastic processes and shows how, due to the experimental constraints, the models converge from the  $\bar{K}N$  threshold on while diverging substantially below it. A direct consequence of the ill-determined  $\bar{K}N$  subthreshold amplitudes, the uncertainty associated to the position of the lower mass  $\Lambda(1405)$  pole becomes very large. More precisely, as can be seen in Fig. 1 and Fig. 6 of Refs. [36, 42] respectively, the different models produce very scattered locations in the complex plane for this pole, while the second pole seems to be very well pinned down since all models provide coordinates gathered around 1420 MeV and with a width of approximately 40 MeV.

In the last years many efforts have been made to improve this situation. This is evidenced by the numerous experiments underway or planned, as well as the theoretical works devoted to this topic that can be found in the literature recently.

With respect to photoproduction experiments, it is worth mentioning the latest GlueX preliminary analysis of the  $\pi^0\Sigma^0$  invariant mass from the  $\gamma p \rightarrow K^+\pi^0\Sigma^0$  process [43], which is in agreement with the previous experimental and theoretical evidences about the double pole structure of the  $\Lambda(1405)$ .

This work was preceded by the theoretical study (and the subsequent extension of the formalism) of  $\gamma p \rightarrow K^+\pi\Sigma$  photoproduction mechanism, in Refs. [44, 45], following an approach that incorporates constraints from unitarity, gauge invariance and chiral perturbation theory.

The next important experimental output will come from the SIDDHARTA-2 high precision measurement of the X-ray of the  $2p$  to  $1s$  transition in kaonic deuterium. The data acquisition campaign is presently ongoing [46]. The combination of this challenging measurement with that of the kaonic hydrogen measurement [22] will provide the isospin-dependent antikaon-nucleon scattering lengths at threshold, which represents a milestone in the exploration of QCD at low energies with strangeness.

Another source of knowledge for the  $\bar{K}N$  interaction below threshold comes from the antineutrino induced  $\Lambda(1405)$  given the relevant role of the strong interaction in the rescattering. This reaction can go via the process  $\bar{\nu}p \rightarrow l^+\phi B$  ( $\phi B$  being a meson-baryon pair), which was theoretically studied in Ref. [47]. On the experimental side, this reaction is one of the possible outputs of the MicroBooNE collaboration, where the role of  $\Lambda$ ,  $\Sigma$  and related hyperon production is currently under analysis. In addition, it is expected that the SBND detector at Fermilab will be able to measure such processes with huge statistics.

The  $K^-d \rightarrow p\Sigma^-$  reaction was suggested in [48] as an alternative window to the  $\bar{K}N$  subthreshold amplitudes. This reaction should take place by means of two triangle topologies which develop a triangle singularity. The authors compute the total cross-section of the process for different  $\bar{K}N$  amplitudes calculated within the UChPT approach. The difference among the different total cross sections is large enough to claim that a future comparison with the experiment could play an important role to discern which models are the most suitable to describe the physics below the  $\bar{K}N$  threshold, with clear implications to pin down the lower mass pole of the  $\Lambda(1405)$ .

In this respect, the Lattice community also makes its contribution providing the simulation on the  $I = 0$  coupled-channel scattering amplitudes of  $\pi\Sigma - \bar{K}N$  [49, 50]. The two-channel K-matrix fitted to the lattice QCD data supported the two-pole picture in agreement with UChPT. Slightly after, a theoretical finite volume analysis based on chiral lagrangians [51] reached a remarkable consistency between the chiral unitary approach predictions for the two-pole structure, the recent LQCD scattering data and the available experimental cross sections. In [52], another theoretical analysis within the renormalizable framework of covariant chiral effective field theory obtained both  $\Lambda(1405)$  poles compatible with those provided by the BaSc Collaboration [49, 50].

The authors of [53] presented a detailed discussion on the lowest-lying  $\frac{1}{2}^-$  and  $\frac{3}{2}^-$   $\Lambda_Q$  resonances ( $Q = s, c, b$ ), paying special attention to the interplay between the conventional quark model (CQM) and chiral baryon-meson degrees of freedom, which are coupled using a unitarized scheme consistent with leading order (LO) heavy quark symmetries. The main conclusion is that the two-pole pattern in the strange sector is a consequence of the decisive role of the  $\bar{K}N$  channel in the dynamics together with the scarce influence of the  $|qqq\rangle$  com-

ponent compared to the corresponding one for the charm and bottom resonances. Ref. [54] contains an interesting analysis of the  $\bar{K}N$  system in the framework of CQM, where the two-pole nature of the  $\Lambda(1405)$  is only recovered when other meson-baryon channels are taken into account via an optical potential. In Ref. [55], the QCD sum rules method was applied and, assuming a molecular pentaquark structure with a  $K^- - p$  and  $\bar{K}^0 - n$  admixture, a mass for the  $\Lambda(1405)$  of  $1406 \pm 128$  MeV was found.

One of the drawbacks that reduces the restrictive effect of the scattering data at energies slightly above the  $K^-p$  threshold is the large uncertainties associated, since the data-taking process went through bubble chambers. In contrast, the precise femtoscopic technique from High-Energy nuclear collisions offers one of the most promising ways to extract information of the hadron-hadron interactions and, in particular, of the  $K^-p$  one. The reason lies in the fact that, for these high-multiplicity event reactions, the hadron production yields are well described by statistical models, thus leaving the correlations between the outgoing particles to depend on the final state scattering. This technique is specially welcome to study the interaction of those sectors where there is no chance to perform scattering experiments due to the short lifetime of the particles involved in the initial state. Therefore, the hadron femtoscopy technique provides an unprecedented opportunity to impose constraints on the theoretical models. Actually, in [56], a novel method to extract information on  $S = -2$  meson-baryon scattering amplitudes was presented employing the  $K^- \Lambda$  correlation function (CF) measured by the ALICE collaboration at LHC [57]. A similar study was carried out in [58] to constrain for the first time the vector meson-baryon scattering amplitude in the  $S = 0, Q = 0$  sector. In line with the former works, yet from the inverse problem perspective, the authors of [59] study several  $S = -1$  meson-baryon CFs to see how much information can be obtained from them focusing on the  $\Sigma^*(1/2^-)$  at the  $N\bar{K}$  threshold.

In the present study, we revisit the  $K^-p$  CF aiming at demonstrating the validity of two benchmark models, developed within the UChPT scheme and constrained to the available scattering data, to reproduce the experimental femtoscopic data. We can say in advance that our conclusions do not support those of [60], claiming a revision of the full coupled-channel  $K^-p$  interaction models in order to properly describe the measured  $K^-p$  CF in relative momentum space obtained in  $pp$  collisions at  $\sqrt{s} = 13$  TeV. Moreover, we provide novel predictions for the  $\pi^- \Lambda$  and  $K^+ \Xi^-$  CFs, whose future comparison to the corresponding ongoing measurements can provide valuable information about the  $S = -1$  meson-baryon interaction not only below the  $\bar{K}N$  threshold but also at higher energies. In all cases, we present a detailed analysis of all the physically meaningful elements of the CFs.

## II. FORMALISM

### A. Femtoscopic correlation function

In the  $S = -1$  sector, different meson-baryon channels with the same quantum numbers couple to each other. In particular, for the charge  $Q = 0$  case we consider ten channels ( $K^-p, \bar{K}^0n, \pi^0\Lambda, \pi^0\Sigma^0, \eta\Lambda, \eta\Sigma^0, \pi^+\Sigma^-, \pi^-\Sigma^+, K^+\Xi^-, K^0\Xi^0$ ), and for  $Q = -1$  we consider six channels ( $\pi^-\Lambda, \pi^0\Sigma^-, \pi^-\Sigma^0, K^-n, \eta\Sigma^-, K^0\Xi^-$ ). In this multichannel scenario, the two-particle CF of the observed  $i$ -channel can be expressed through the generalized Koonin-Pratt formula [61, 62], which has been recently reinforced by the study presented in [63],

$$C_i(p) = \sum_j w_j \int d^3r S_j(r) |\Psi_{ji}(p, r)|^2. \quad (1)$$

The variables  $p$  and  $r$  represent the relative momentum and distance between the two particles observed in the pair rest frame, respectively. The preceding summation covers the possible transitions allowed by the theory at hand from all possible  $j$ -particle pairs to the final  $i$ -pair. These  $j$ -contributions are scaled by the so-called production weights,  $w_j$ , accounting for the amount of primary pairs  $j$  produced in the initial  $pp$  collision, that can transform into the measured final  $i$ -pair in a region of  $p$  below 200 MeV/c. The calculation of the production weights is performed following the same approach used in the  $K^-p$  ALICE measurement [60] and in the recent study of the  $K^- \Lambda$  correlation in [56] (see its Supplemental Material for details). The corresponding  $w_j$ 's entering in the different CFs studied in this work are displayed in Table I. As expected, we obtain a significant increase in the value of the production weights involving pions for the  $K^+ \Xi^-$  system due to the lower yields of  $\Xi$  baryons with respect to light hadrons. It follows that for the  $\pi^- \Lambda$  pairs we indeed observe the opposite trend, with all the  $j$  weights well below unity.

The source function,  $S_j(r)$ , stands for the emitting source, and represents the probability distribution of producing the  $j$ -th pair at a relative distance  $r$ . For CFs measured in  $pp$  collisions at LHC energies, the ALICE Collaboration showed that the emitting source is composed of a Gaussian core, common to all particles, and a non-Gaussian component coming from strongly decaying resonances into the particles forming the pair of interest [64, 65]. In particular, the core source size  $r_{\text{core}}$  depends on the average transverse mass  $\langle m_T \rangle$  of the pair under study. This core-resonance halo source function is typically parametrized as an effective spherical Gaussian,  $S_j(r) = (4\pi R_j^2)^{-3/2} \exp(-r^2/4R_j^2)$ , with size  $R_j$ . The latter can depend on the channel due to the different feed-down of strongly decaying resonances into the particles composing each  $j$  pair.

For the  $K^-p$  CF, we employed the source sizes reported in [60]:  $R_{\bar{K}N} = 1.08 \pm 0.18$  fm and  $R_{\pi\Sigma, \pi\Lambda} = 1.23 \pm 0.21$  fm<sup>1</sup>.

<sup>1</sup> We report the total uncertainty evaluated as the squared root of the sum in

Since in that work the  $\eta\Lambda$ ,  $\eta\Sigma^0$ ,  $K^+\Xi^-$  and  $K^0\Xi^0$  channels were not included, their corresponding source sizes are fixed to 1.25 fm. As will be shown later, these channels have a negligible contribution to the  $K^-p$  CF and thus the possible variation of their source sizes does not affect our results. For the  $K^+\Xi^-$  and  $\pi^-\Lambda$  CFs no experimental information is yet available, and the same source size is used for every channel, presenting three cases:  $R = 1.0$  fm,  $R = 1.25$  fm and  $R = 1.5$  fm.

Finally, the last ingredient in the former expression,  $\Psi_{ji}(p, r)$ , is the relative wave function of the pair and contains the information of the interaction. Following [66], the relative wave function can be obtained directly from the scattering amplitude by solving a BS equation.

## B. Strong interaction

In order to model the meson-baryon strong interaction in the  $S = -1$  sector, as already mentioned in the Introduction, we employ a UChPT scheme within a coupled-channels formalism. We obtain the scattering amplitude starting from the effective chiral Lagrangian up to NLO,  $\mathcal{L}_{\phi\mathcal{B}} = \mathcal{L}^{(1)} + \mathcal{L}^{(2)}$ , given by

$$\begin{aligned} \mathcal{L}^{(1)} &= \langle \bar{B}i\gamma^\mu D_\mu B \rangle - M_0 \langle \bar{B}B \rangle + \frac{1}{2} D \langle \bar{B}\gamma^\mu \gamma^5 \{u_\mu, B\} \rangle \\ &+ \frac{1}{2} F \langle \bar{B}\gamma^\mu \gamma^5 [u_\mu, B] \rangle, \end{aligned} \quad (2)$$

$$\begin{aligned} \mathcal{L}^{(2)} &= b_D \langle \bar{B}\{\chi_+, B\} \rangle + b_F \langle \bar{B}[\chi_+, B] \rangle + b_0 \langle \bar{B}B \rangle \langle \chi_+ \rangle \\ &+ d_1 \langle \bar{B}\{u_\mu, [u^\mu, B]\} \rangle + d_2 \langle \bar{B}[u_\mu, [u^\mu, B]] \rangle \\ &+ d_3 \langle \bar{B}u_\mu \rangle \langle u^\mu B \rangle + d_4 \langle \bar{B}B \rangle \langle u^\mu u_\mu \rangle. \end{aligned} \quad (3)$$

Here,  $B$  is the octet baryon matrix, while the pseudoscalar mesons matrix  $\phi$  is contained in the field  $u_\mu = iu^\dagger \partial_\mu U u^\dagger$ , where  $U = u^2 = \exp(i\sqrt{2}\phi/f)$  and  $f$  is the effective meson decay constant. The covariant derivative is defined as  $D_\mu B = \partial_\mu B + [\Gamma_\mu, B]$ , where  $\Gamma_\mu = (u^\dagger \partial_\mu u + u \partial_\mu u^\dagger)/2$ , and  $\chi_+ = -\{\phi, \{\phi, \chi\}\}/4f^2$ , where  $\chi = \text{diag}(m_\pi^2, m_\pi^2, m_K^2 - m_\pi^2)$ . This Lagrangian depends on the axial vector constants  $D$  and  $F$ , together with  $f$  and the NLO LECs ( $b_D, b_F, b_0, d_1, d_2, d_3, d_4$ ).

The interaction kernel is obtained from Eqs. (2) and (3) projecting the resulting potential onto its  $L = 0$  partial wave and averaging over polarization states,

$$V_{ij}(\sqrt{s}) = \frac{1}{8\pi} \sum_{\sigma, \sigma'} \int d\Omega \hat{V}_{ij}(\sqrt{s}, \Omega, \sigma, \sigma') \quad (4)$$

where  $V_{ij}$  represent the different interaction kernel matrix elements associated to the transitions from the incoming  $i$ -th to the outgoing  $j$ -th channels. The interaction kernel can be separated into four contributions: the Weinberg-Tomozawa

(WT) calculated from the covariant derivative, direct Born and crossed Born terms, whose vertices are obtained from the last 2 terms of  $\mathcal{L}^{(1)}$ , and the NLO terms at tree level, derived from  $\mathcal{L}^{(2)}$ . These contributions are depicted diagrammatically in Fig. 1. For more details on the explicit form of these contributions see [35, 67].

Unitarity is implemented into the scheme via the BS equations, whose solution leads to scattering amplitudes. Within the on-shell approximation [7, 27] the BS equations can be written in the matrix form

$$T = (1 - VG)^{-1}V \quad (5)$$

where  $G$  is a diagonal matrix whose elements are the meson-baryon loop functions, which diverge logarithmically and, therefore, have to be regularized. Following the dimensional regularization (DR) method, its diagonal elements can be expressed as

$$\begin{aligned} G_l(\sqrt{s}) &= \frac{2M_l}{16\pi^2} \left[ a_l(\mu) + \ln \frac{M_l^2}{\mu^2} + \frac{m_l^2 - M_l^2 + s}{2s} \ln \frac{m_l^2}{M_l^2} \right. \\ &\left. + \frac{q_l}{\sqrt{s}} \ln \frac{(s + 2q_l\sqrt{s})^2 - (M_l^2 - m_l^2)^2}{(-s + 2q_l\sqrt{s})^2 - (M_l^2 - m_l^2)^2} \right] \end{aligned} \quad (6)$$

where  $M_l$  and  $m_l$  are, respectively, the baryon and meson masses of the  $l$ -th channel and  $q_l$  the center of mass (CM) momentum of the  $l$ -th channel pair at a  $\sqrt{s}$  energy. The  $a_l$  are the so-called subtraction constants (SCs), which replace the divergence for a given regularization scale  $\mu$ . In principle, there are as many SCs as channels taken into account in the considered sector, but the number of SCs can be reduced assuming isospin-symmetry arguments for the elements of each channel multiplet.

Throughout this work we employ two models. On the one hand, the Oset-Ramos model [14] that is based on an interaction kernel consisting of the WT contribution and is regularized via DR thereby depending on 7 free parameters, namely the decay constant  $f$  and 6 SCs (one for each meson-baryon channel, taking isospin symmetry into account). On the other hand, the BCN model [36] which employs the full interaction kernel from Eqs. (2) and (3), and thus depends on 16 free parameters (10 LECs and 6 SCs).

## C. Coulomb interaction

For the  $Q = 0$  case, besides the strong interaction, one must take into account the Coulomb one. Following [68], the  $s$ -wave component of the Coulomb interaction kernel is

$$\begin{aligned} V^c(\varepsilon, p, p') &= \frac{2\pi\varepsilon\alpha}{pp'} \left\{ Ci[|p' - p|R_c] - Ci[(p' + p)R_c] \right. \\ &\left. + \ln \frac{(p' + p)R_c}{|p' - p|R_c} \right\} \end{aligned} \quad (7)$$

where  $Ci[x] = \int_x^\infty dt \cos(t)/t$  is the cosine integral function,  $\varepsilon = \pm 1$  is the signature of the interaction and  $\alpha$  the fine structure constant. The parameter  $R_c$ , chosen to be 60 fm, is introduced to truncate the Fourier transform of the Coulomb potential and thus avoid the divergence at  $p' = p$ .

---

quadrature of the statistical and systematic experimental errors.

channel- $j$	$w_j (K^- p \text{ CF})$	$w_j (K^+ \Xi^- \text{ CF})$	channel- $j$	$w_j (\pi^- \Lambda \text{ CF})$
$K^- p$	1	$13.26 \pm 0.32$	$\pi^- \Lambda$	1
$\bar{K}^0 n$	$0.97 \pm 0.20$ [60]	$12.85 \pm 0.29$	$\pi^0 \Sigma^-$	$0.70 \pm 0.02$
$\pi^0 \Lambda$	$1.96 \pm 0.93$ [60]	$26.40 \pm 2.33$	$\pi^- \Sigma^0$	$0.69 \pm 0.01$
$\pi^0 \Sigma^0$	$1.37 \pm 0.68$ [60]	$18.01 \pm 1.48$	$K^- n$	$0.48 \pm 0.06$
$\pi^+ \Sigma^-$	$1.42 \pm 0.71$ [60]	$15.92 \pm 1.29$	$\eta \Sigma^-$	$0.08 \pm 0.01$
$\pi^- \Sigma^+$	$1.41 \pm 0.70$ [60]	$16.56 \pm 1.35$	$K^0 \Xi^-$	$0.04 \pm 0.01$
$\eta \Lambda$	$0.25 \pm 0.01$	$3.34 \pm 0.02$	-	-
$\eta \Sigma^0$	$0.17 \pm 0.01$	$2.29 \pm 0.01$	-	-
$K^+ \Xi^-$	0.08	1	-	-
$K^0 \Xi^0$	0.08	1.01	-	-

TABLE I. Values of the production weights for  $\pi^- \Lambda$ ,  $K^- p$  and  $K^+ \Xi^-$  CFs.

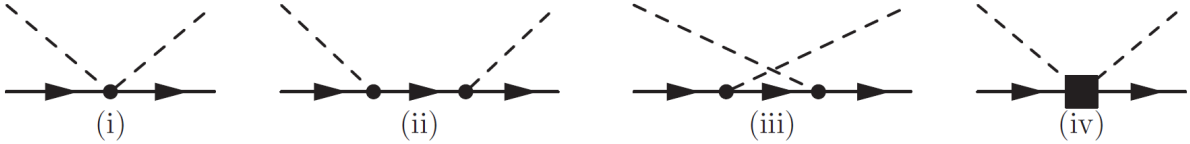


FIG. 1. Diagrammatic contributions to the interaction kernel. Contact diagrams (i) and (iv) represent the WT and NLO terms, respectively. Diagrams (ii) and (iii) represent the direct Born (s-channel) and the crossed Born (u-channel) terms, respectively.

A common procedure would consist in unitarizing simultaneously the combined strong and Coulomb amplitudes, within a cut-off regularization scheme, as done in [68]. However, the strong interaction models explored in the present work have been fitted to the scattering observables employing the DR unitarization scheme. Applying a cut-off unitarization scheme would modify the predictions of the scattering observables, hence requiring a refitting of the models, which is not the purpose of the present work. We recall that we aim at exploring the ability of the meson-baryon interaction models (constrained to the scattering data in the strangeness  $S = -1$  sector) in reproducing the  $K^- p$  correlation function, as well as showing predictions for the  $\pi^- \Lambda$  and  $K^+ \Xi^-$  correlation functions in the same sector. Therefore, to avoid modifying the already tuned strong amplitudes, we opt for obtaining the total scattering amplitude as

$$T_{ij}(\sqrt{s}, p, p') = T_{ij}^S(\sqrt{s}) + \delta_{ij} T_{ii}^c(\sqrt{s}, p, p') \quad (8)$$

where  $T^S$  is the strong scattering amplitude obtained in section II B and  $T^c(\sqrt{s}, p, p') = \tilde{V}^c(\sqrt{s}, p, p')$  is the Coulomb one up to first order in the BS equation<sup>2</sup>. Here,  $\tilde{V}^c$  is obtained from  $V^c$  applying correction factors for it to match the relativistic

structure of the strong amplitude. Namely,

$$\begin{aligned} \tilde{V}_{ii}^c(\sqrt{s}, p, p') &= \sqrt{\frac{E_i(p)}{M_i}} \sqrt{2\omega_i(p)} \sqrt{\xi(p, s)} \times V^c(\varepsilon, p, p') \\ &\times \sqrt{\xi(p', s)} \sqrt{2\omega_i(p')} \sqrt{\frac{E_i(p')}{M_j}} \end{aligned} \quad (9)$$

where  $E_i$  and  $M_i$  are the energy and mass of the baryon,  $\omega_i$  the energy of the meson and

$$\xi(p, s) = \frac{\sqrt{s} - E(p) - \omega(p)}{(p^0)^2/2\mu - p^2/2\mu} \quad (10)$$

with  $\mu$  the pair's reduced mass and  $p^0$  the CM momentum associated to an energy  $\sqrt{s}$ .

### III. RESULTS

In this section we present the results obtained for each CF separately. Apart from providing a prediction for the different CFs employing the Oset-Ramos and BCN models, we delve deeper into the relevance of the contributing terms in the interaction kernel. Furthermore, we show the role of each transition  $\psi_{j,i}(p, r)$  for the corresponding CF. We start computing  $C_i(p)$  taking into account only the elastic  $\psi_{i,i}$  and, following Eq. (1), we progressively add the other channel contributions. Despite the Oset-Ramos model provides an overall good description of the available  $\bar{K}N$  data, a special attention is paid to the BCN model given the great accuracy shown in describing such data thanks to the incorporation of higher order corrections in the kernel.

<sup>2</sup> We have numerically checked that solving the BS equation with the combined strong and Coulomb interactions (employing cut-off values in the range 600 – 1200 MeV) gives a CF that does not differ much from the sum of the separately unitarized amplitudes shown in Eq. 8, the difference lying well within the error bands explored in this work. We have also checked that the first order Coulomb amplitude is practically indistinguishable from the fully unitarized one.

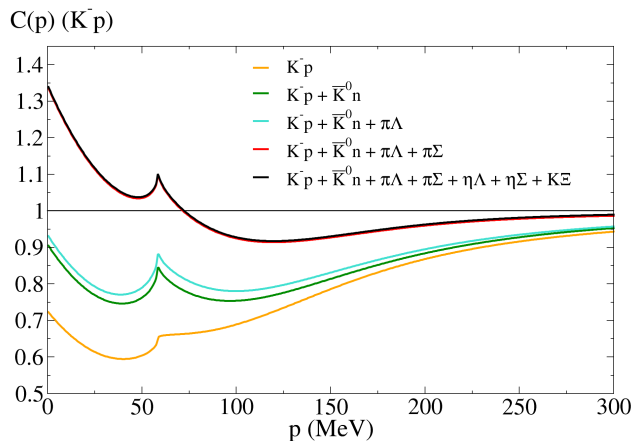


FIG. 2. Contribution of the different transitions to the  $K^- p$  CF.

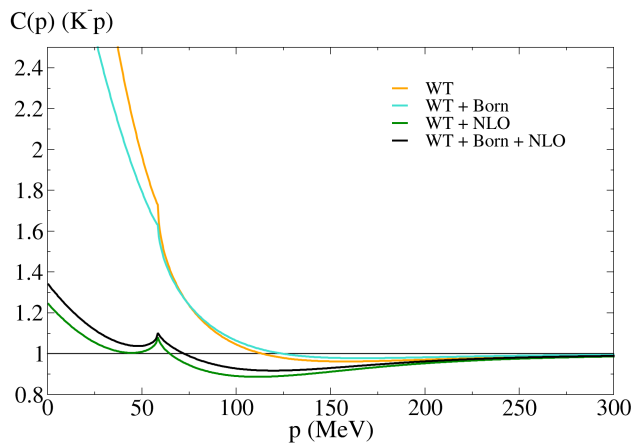


FIG. 3. Contribution of the different interaction-kernel terms into the  $K^- p$  CF.

### A. $K^- p$ correlation

In the first place, the coupled-channel relevance in the  $K^- p$  CF can be appreciated in Fig. 2. From the ochre line, one immediately realizes that the elastic transition is not able to reproduce by itself the experimental data (see Fig. 4). From Fig. 2, it can be also noted that the  $\bar{K}^0 n, \pi\Lambda, \pi\Sigma$  channels contribute to the total  $C_{K^- p}(p)$  to a greater or lesser extent depending on their interplay and on the penalizing production weight. These are notably lower for the heavier channels compared to the lighter pseudoscalar-baryon pairs, thereby making the  $\eta\Lambda, \eta\Sigma, K\Xi$  channels to barely contribute (see second column of Table I). One of the achievements of the measured  $K^- p$  CF [69] is the observation of a structure around a relative momentum of  $p = 58$  MeV/c that constitutes the first experimental evidence for the opening of the  $\bar{K}^0 n$  channel. This signature cusp structure is clearly seen in the different contributions of Fig. 2 as a clear consequence of the coupled-channel effects arising from the unitarization.

In Fig. 3, the role of the different pieces contributing to the

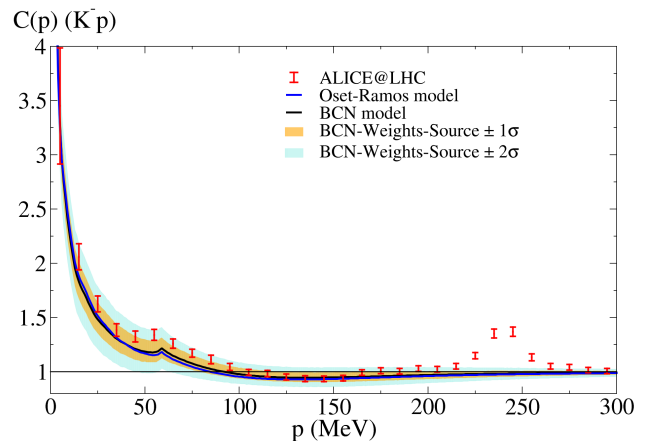


FIG. 4.  $K^- p$  CFs for the BCN and Oset-Ramos models (black and blue lines respectively), as well as the error bands associated to BCN model (see details in the text). The experimental data points are taken from [60] ( $p-p$  collision data set at  $\sqrt{s} = 13$  TeV in Fig.4).

interaction kernel of the BCN model is addressed. The green line, which represents what one gets when dealing with an interaction kernel obtained out of the WT+NLO terms, shows the dominance of both former terms in the  $C_{K^- p}(p)$ . The comparison between the black line, accounting for the full kernel, and the green one reveals the mere fine tuning role of the Born terms for this CF. What becomes clear from this plot is the intricate mechanism behind the UChPT formalism that allows the interplay between the different channels through the different kernel terms providing a counterintuitive interference pattern beyond a plain addition of corrections on the dominant contact term.

Fig. 4 contains the  $K^- p$  CFs obtained from the two models combined with the Coulomb interaction. Both models reach an overall good description of the CF data along the momentum range, excluding the structure corresponding to the  $\Lambda(1520)$ , with  $J^P = 3/2^-$ , which cannot be reproduced by the bare theoretical model since it is limited to s-wave. Actually, the slightly major strength of the BCN model (black line) qualifies it to improve in the description of the experimental data. However, in the momentum range going from 45 to 90 MeV/c, the theoretical models slightly underestimate the experimental data. Nevertheless, once the associated errors<sup>3</sup> are taken into account, one can appreciate that the experimental data is well described, which gives us confidence in the soundness of the BCN model. We would like to highlight that the error associated to the source sizes  $R_j$  is the main source

<sup>3</sup> To estimate the error bands we randomly sample the values of the parameters needed to calculate the CF (LECs, SCs,  $w_j$ 's and  $R_j$ 's) within  $1\sigma$  or  $2\sigma$  associated uncertainty obtaining a complete parametrization. We iterate the process thousand times thereby getting the corresponding thousand sets of parameters. With these, we calculate the thousand CFs for 100 values of the momentum. Afterwards, from the normal distributions around each momentum value, we extract the standard deviation for each given momentum value.

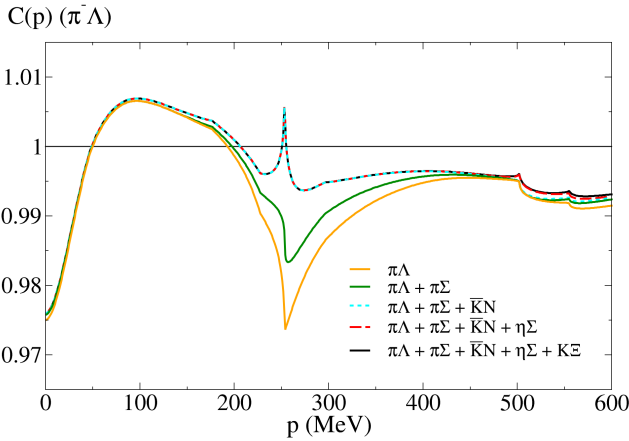


FIG. 5. Contribution of the different transitions to the  $\pi^- \Lambda$  CF for a source size  $R = 1.25$  fm.

of uncertainty for the CFs [64, 65, 70].

In Ref. [60], for the analogous case in  $p-p$  collisions, the authors compare a theoretical  $K^- p$  CF, calculated from the chirally motivated potentials of [71], with the same experimental data we report in Fig. 4. By assuming the production weights, up to the  $\pi^- \Sigma^+$  channel, fixed to the values reported in Tab. I and the same sources mentioned in Sec. II, the modeled CFs largely underestimate the data in a much wider momentum range [20, 90] MeV/c (blue band in Fig. 4 of Ref. [60]). A better description of the data is achieved only if the  $w_{\bar{K}^0 n}$  weight is enhanced of roughly a factor 2. This fact leads the authors to claim that the CF data measured in Ref. [69] provide a unique constraint to pin down the coupling strength to the  $\bar{K}^0 n$  channel. In our opinion, this is a too strong statement, as it has been shown above. On the contrary, the BCN model, already able to nicely reproduce the scattering data, does also a good job in reproducing the cusp region of the CF, showing in an indirect way the full compatibility between scattering and CF data.

### B. $\pi^- \Lambda$ correlation

We now analyze the  $\pi^- \Lambda$  CF following the same scheme as in the previous case. Before moving on to the decomposition in terms of the different channel transitions, it is worth reminding that this CF, once measured, can provide novel information about  $\bar{K} N$  subthreshold amplitudes. An important fact to be considered is the null elastic transition for the dominant contact term. Actually, the only surviving WT contributions are the  $K^- n \rightarrow \pi^- \Lambda$  and  $K^0 \Xi^- \rightarrow \pi^- \Lambda$  transitions (as can be inferred from Table I in [7]), which is reflected by the remarkable enhancement of the cyan line, due to the  $K^- n$  opening, with respect to the green one in Fig. 5<sup>4</sup>. The limited relevance

<sup>4</sup> Similar enhancement would be seen once the  $K^0 \Xi^- \rightarrow \pi^- \Lambda$  transition was incorporated into the CF. However, the tiny value for the corresponding

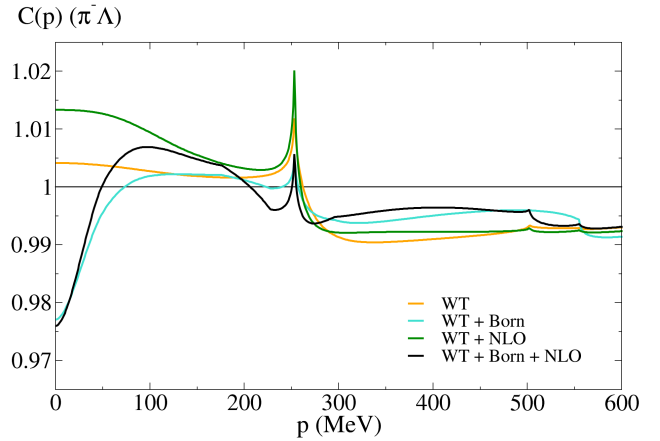


FIG. 6. Contribution of the different interaction-kernel terms to the  $\pi^- \Lambda$  CF for a source size  $R = 1.25$  fm.

of the WT terms confers a dominant character to the Born and NLO terms as well as the coupled-channel effect. This is the reason for the small deviation from one shown by the  $\pi^- \Lambda$  CFs obtained for the different combinations of the interaction kernel terms, as can be noted from the y-axis scale in Fig. 6. There, from the discrepancies at lower momenta, one appreciates a sizable contribution from the Born terms evidenced by the reduction of the black line (obtained with the full kernel) with respect to the green line (obtained when building the interaction from the WT+NLO terms). Regarding the opening thresholds, apart from the above-mentioned  $K^- n$  one, we can appreciate the ones corresponding to the  $\eta \Sigma^-$  and  $K^0 \Xi^-$  channels. On the other hand, no trace of the  $\pi \Sigma$  openings because the  $\pi^- \Lambda \rightarrow \pi \Sigma$  transitions can only proceed via the Born terms which provide a negligible contribution around the  $\pi \Sigma$  threshold<sup>5</sup>.

Finally, in Fig. 7, we display the comparison of the obtained  $\pi^- \Lambda$  CF employing the BCN and Oset-Ramos models for different source size radii ( $R = 1, 1.25, 1.5$  fm). The lack of many contributions coming from the WT term in this sector, which is the only one considered in the Oset-Ramos model, makes the corresponding CF to be quite featureless, except for the cusp at the  $K^- n$  opening. In contrast, the BCN model has a richer pattern of contributions intertwined by the coupled-channel formalism, as already said above, hence producing a substantial drop in the  $\pi^- \Lambda$  CF at low relative momenta. We can also observe that, as the source size increases, both models acquire a smoother behavior and the discrepancies between them become progressively smaller as expected. We also include the quite sizeable error bands corresponding to the BCN model, which diminishes the discrepancies between both models at low momenta. For completeness, we also show

$\omega_{K^0 \Xi^-}$  prevents it effectively (see the last column in Table I).

<sup>5</sup> The null contribution of the WT and the NLO terms in the  $\pi^- \Lambda \rightarrow \pi \Sigma$  transitions can be explained by the zero value of the corresponding couplings, as shown in Tables VII and VIII of Ref. [34]

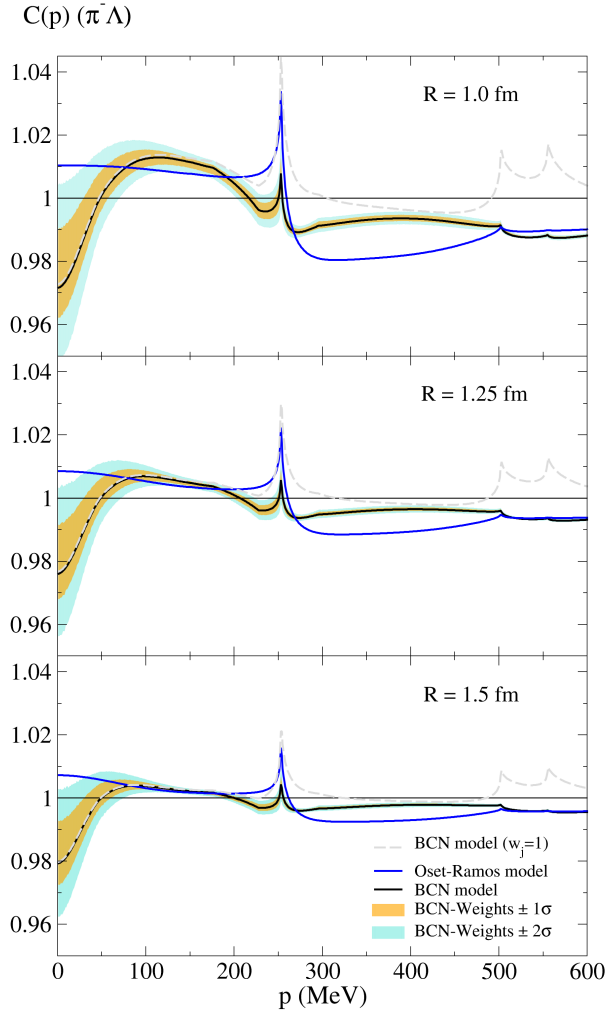


FIG. 7.  $\pi^- \Lambda$  CFs for the BCN and Oset-Ramos models (black and blue lines respectively), as well as the error bands associated to BCN model (see details in the text), for three values of the source size  $R$ . Dashed gray line shows the CF setting all the production weights to unity.

in Fig. 7 the  $\pi^- \Lambda$  CF when taking all weights  $w_j = 1$  (gray dashed line). This is done in order to provide a baseline for future comparisons with the experimental data, since some of the extrapolations carried out in the calculation of the production weights can be slightly modified because of the  $\pi^- \Lambda$  threshold, whose location is far below in the energy range.

### C. $K^+ \Xi^-$ correlation

Lastly, we present our prediction for the  $K^+ \Xi^-$  CF. The coupled-channel contributions are shown in Fig. 8. Besides the elastic channel, we observe that the most sizable contribution is that of the  $\pi \Lambda$  channel, whose production weight is also the largest (see Table I), followed by those of the  $\pi \Sigma$  and  $\eta \Lambda$  ones. Note that, in spite of the  $K^- p$  and  $\bar{K}^0 n$  weights being

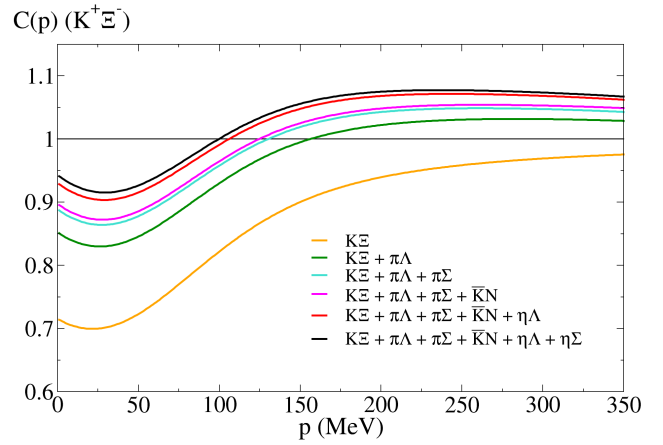


FIG. 8. Contribution of the different transitions to the  $K^+ \Xi^-$  CF for a source size  $R = 1.25$  fm.

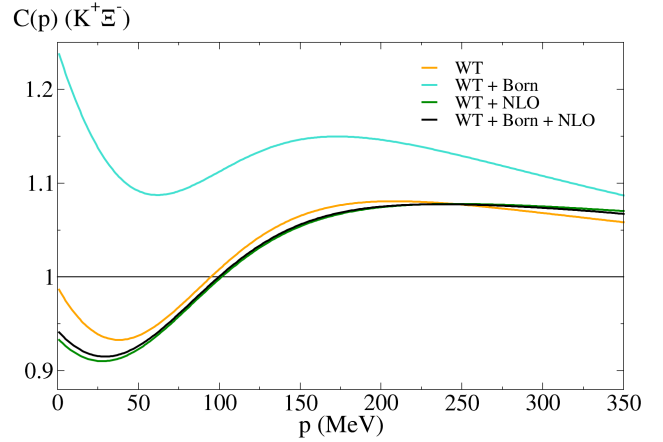


FIG. 9. Contribution of the different interaction-kernel terms to the  $K^+ \Xi^-$  CF for a source size  $R = 1.25$  fm.

much larger than that of the  $\eta \Lambda$  channel, their contribution is almost negligible due to the vanishing WT coefficients of the  $\bar{K} N \rightarrow K^+ \Xi^-$  transitions and the almost zero NLO ones<sup>6</sup>.

Fig. 9 shows the contribution of the different pieces of the interaction kernel of the BCN model to the  $K^+ \Xi^-$  CF. Although the combination of the WT and NLO terms apparently describes the full CF without the need of the Born ones, the cyan line shows the importance of these terms when they are combined with the WT contribution. Thus, this channel shows the importance of the interplay between the Born terms and the rest of the interaction kernel, which could not be appreciated in the  $K^- p$  case. This fact does not come as a novelty, since it is expected from the findings of Ref. [35].

In Fig. 10 the full  $K^+ \Xi^-$  CF is shown, which takes into ac-

<sup>6</sup> This can be understood by considering the expressions of the WT and NLO kernels in Eqs. (2) and (3), taking the values of the preceding coefficients from Table II in Ref. [36].



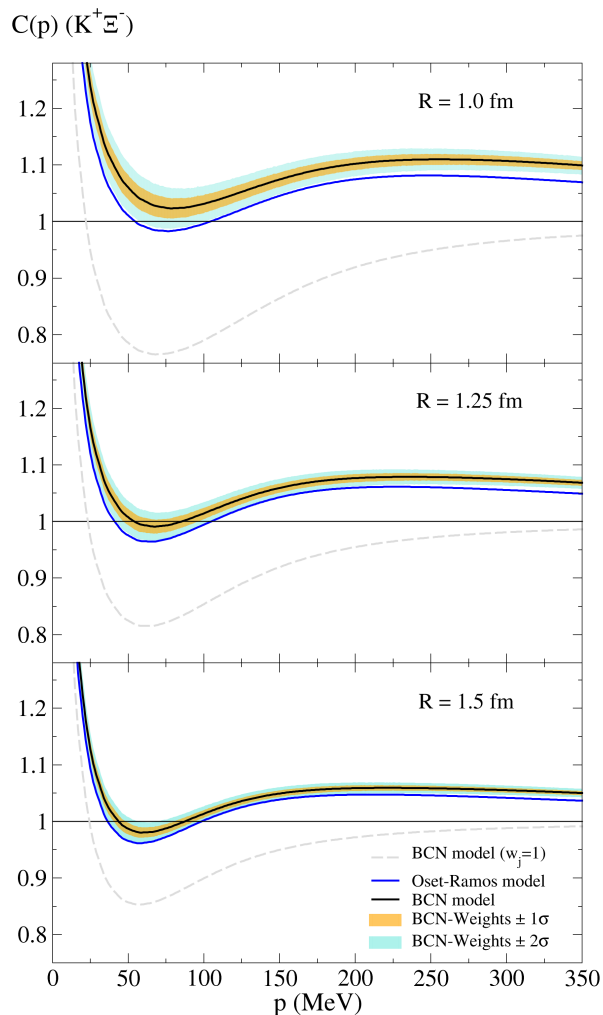


FIG. 10.  $K^+\Xi^-$  CFs for the BCN and Oset-Ramos models (black and blue lines respectively), as well as the error bands associated to BCN model (see details in the text), for three values of the source size  $R$ . Dashed gray line shows the CF setting all the production weights to unity.

count the strong contribution predicted by the BCN and Oset-Ramos models combined with the Coulomb interaction. The errorbands correspond to the propagated uncertainties of the BCN model parameters and the production weights of Table I. Due to the lack of experimental information of the source associated to this channel, a Gaussian source is assumed for every channel. To show the dependence of the CF on the source size, three different radii are displayed within the scope of reasonable source sizes in p-p collisions. It can be seen that both models give a similar description, although the availability of experimental data could set a substantial difference between both predictions. For the reasons stated above, we also include a gray dashed line obtained when fixing all the production weights to 1 in the  $K^+\Xi^-$  CF. In this last case, it can be clearly appreciated the reduction of the influence of the lighter channels. Actually, this correlation function is currently under

experimental analysis by ALICE, which opens the possibility of accessing energies where information obtained through scattering experiments is scarce.

#### IV. CONCLUSIONS

We have carried out a detailed study of the correlation functions for three meson-baryon pairs in the  $S = -1$  sector. In all cases, we employed UChPT based models in coupled-channel as inputs to calculate the corresponding CFs. In particular, we focus on the BCN model that has been constrained to many different observables and showed a notable predictive power in this sector. This work has also been complemented not only by a comprehensive analysis of the role played by each channel in the corresponding CF but also by the relevance of the different contributions in the interaction kernel.

First, we revisited the  $K^-p$  CF with available experimental data and already analyzed theoretically in the existing literature. In contrast to the previous analysis, we showed that the BCN model is capable to describe the experimental data within  $1\sigma$  discrepancy, thereby dispelling any doubt about the reliability of the current chiral models to describe the meson-baryon interactions in this sector. As a matter of fact, our result is indirectly demonstrating the compatibility among the scattering cross-sections, the measurement of the  $\bar{K}N$  threshold observables and the femtoscopic data. This fact gives us confidence in the potential of the femtoscopy technique to provide future constraints on theoretical scattering amplitudes, especially for those transitions where scattering experiments are not feasible.

We have also provided, for the first time, predictions for the  $K^+\Xi^-$  and the  $\pi^-\Lambda$  CFs with the corresponding estimation of the error bands considering the uncertainties of the model parameters and the errors associated to the production weights. Such observables are currently under analysis by the ALICE collaboration, whose future comparison with the theoretical predictions will certainly shed some light on the almost uncharted meson-baryon interaction below the  $\bar{K}N$  threshold and provide valuable insights at higher energies, where the available  $K^-p \rightarrow K\Xi$  cross section data have associated large uncertainties.

We are just at the beginning of the LHC RUN3 data taking in a higher precision era and it is most probable that exciting outputs will be obtained in the near future. The interpretation of the experiments and the subsequent studies to learn about the nature of the  $\bar{K}N$  interaction is a task that will require the combined efforts of both experimentalists and theoreticians, to which the present work aims at contributing.

#### ACKNOWLEDGMENTS

P. E. is supported by the Spanish Ministerio de Ciencia e Innovación (MICINN) and European FEDER funds under Contracts No. PID2020-112777GB-I00, PID2023-147458NB-C21 and CEX2023-001292-S (Unidad de Excelencia ‘‘Severo Ochoa’’); by Generalitat Valenciana under

contract CIPROM/2023/59. A. R. acknowledges support from MICIU/AEI/10.13039/501100011033 and by FEDER UE through grant PID2023-147112NB-C21 and through the “Unit of Excellence María de Maeztu 2020-2023” award to the Institute of Cosmos Sciences, grant CEX2019-000918-M.

A. F. was supported by ORIGINS cluster DFG under Germany’s Excellence Strategy-EXC2094 - 390783311 and the DFG through the Grant SFB 1258 “Neutrinos and Dark Matter in Astro and Particle Physics”. V. M. S. was supported by the Deutsche Forschungsgemeinschaft (DFG) through the grant MA 8660/1 – 1.

- 
- [1] R. H. Dalitz and S. F. Tuan, *Annals Phys.* **10**, 307 (1960).
- [2] E. A. Veit, B. K. Jennings, R. C. Barrett, and A. W. Thomas, *Phys. Lett. B* **137**, 415 (1984).
- [3] P. J. Fink, Jr., G. He, R. H. Landau, and J. W. Schnick, *Phys. Rev. C* **41**, 2720 (1990).
- [4] G.-I. He and R. H. Landau, *Phys. Rev. C* **48**, 3047 (1993), arXiv:nucl-th/9308003.
- [5] N. Kaiser, P. B. Siegel, and W. Weise, *Nucl. Phys. A* **594**, 325 (1995), arXiv:nucl-th/9505043.
- [6] N. Kaiser, T. Waas, and W. Weise, *Nucl. Phys. A* **612**, 297 (1997), arXiv:hep-ph/9607459.
- [7] E. Oset and A. Ramos, *Nucl. Phys. A* **635**, 99 (1998), arXiv:nucl-th/9711022.
- [8] J. A. Oller and U. G. Meissner, *Phys. Lett. B* **500**, 263 (2001), arXiv:hep-ph/0011146.
- [9] M. F. M. Lutz and E. E. Kolomeitsev, *Nucl. Phys. A* **700**, 193 (2002), arXiv:nucl-th/0105042.
- [10] B. Borasoy, E. Marco, and S. Wetzel, *Phys. Rev. C* **66**, 055208 (2002), arXiv:hep-ph/0212256.
- [11] C. Garcia-Recio, J. Nieves, E. Ruiz Arriola, and M. J. Vicente Vacas, *Phys. Rev. D* **67**, 076009 (2003), arXiv:hep-ph/0210311.
- [12] A. Bahaoui, C. Fayard, T. Mizutani, and B. Saghai, *Phys. Rev. C* **68**, 064001 (2003), arXiv:nucl-th/0307067.
- [13] B. Borasoy, R. Nissler, and W. Weise, *Eur. Phys. J. A* **25**, 79 (2005), arXiv:hep-ph/0503043.
- [14] D. Jido, J. A. Oller, E. Oset, A. Ramos, and U. G. Meissner, *Nucl. Phys. A* **725**, 181 (2003), arXiv:nucl-th/0303062.
- [15] V. K. Magas, E. Oset, and A. Ramos, *Phys. Rev. Lett.* **95**, 052301 (2005), arXiv:hep-ph/0503043.
- [16] R. H. Dalitz and S. F. Tuan, *Annals Phys.* **8**, 100 (1959).
- [17] S. Navas *et al.* (Particle Data Group), *Phys. Rev. D* **110**, 030001 (2024).
- [18] B. Borasoy, U. G. Meissner, and R. Nissler, *Phys. Rev. C* **74**, 055201 (2006), arXiv:hep-ph/0606108.
- [19] I. Zychor *et al.*, *Phys. Lett. B* **660**, 167 (2008), arXiv:0705.1039 [nucl-ex].
- [20] G. Agakishiev *et al.* (HADES), *Phys. Rev. C* **87**, 025201 (2013), arXiv:1208.0205 [nucl-ex].
- [21] K. Moriya *et al.* (CLAS), *Phys. Rev. Lett.* **112**, 082004 (2014), arXiv:1402.2296 [hep-ex].
- [22] M. Bazzi *et al.* (SIDDHARTA), *Phys. Lett. B* **704**, 113 (2011), arXiv:1105.3090 [nucl-ex].
- [23] G. Beer *et al.* (DEAR), *Phys. Rev. Lett.* **94**, 212302 (2005).
- [24] M. Cargnelli *et al.* (DEAR), *Int. J. Mod. Phys. A* **20**, 341 (2005).
- [25] M. Iwasaki *et al.*, *Phys. Rev. Lett.* **78**, 3067 (1997).
- [26] Y. Ikeda, T. Hyodo, and W. Weise, *Nucl. Phys. A* **881**, 98 (2012), arXiv:1201.6549 [nucl-th].
- [27] T. Hyodo and D. Jido, *Prog. Part. Nucl. Phys.* **67**, 55 (2012), arXiv:1104.4474 [nucl-th].
- [28] A. Cieply and J. Smejkal, *Nucl. Phys. A* **881**, 115 (2012), arXiv:1112.0917 [nucl-th].
- [29] Z.-H. Guo and J. A. Oller, *Phys. Rev. C* **87**, 035202 (2013), arXiv:1210.3485 [hep-ph].
- [30] T. Mizutani, C. Fayard, B. Saghai, and K. Tsushima, *Phys. Rev. C* **87**, 035201 (2013), arXiv:1211.5824 [hep-ph].
- [31] L. Roca and E. Oset, *Phys. Rev. C* **87**, 055201 (2013), arXiv:1301.5741 [nucl-th].
- [32] L. Roca and E. Oset, *Phys. Rev. C* **88**, 055206 (2013), arXiv:1307.5752 [nucl-th].
- [33] M. Mai and U.-G. Meißner, *Eur. Phys. J. A* **51**, 30 (2015), arXiv:1411.7884 [hep-ph].
- [34] A. Feijoo, V. K. Magas, and A. Ramos, *Phys. Rev. C* **92**, 015206 (2015), arXiv:1502.07956 [nucl-th].
- [35] A. Ramos, A. Feijoo, and V. K. Magas, *Nucl. Phys. A* **954**, 58 (2016), arXiv:1605.03767 [nucl-th].
- [36] A. Feijoo, V. Magas, and A. Ramos, *Phys. Rev. C* **99**, 035211 (2019), arXiv:1810.07600 [hep-ph].
- [37] K. Piscicchia *et al.*, *Phys. Lett. B* **782**, 339 (2018).
- [38] M. Amaryan, E. Chudakov, C. Meyer, M. Pennington, J. Ritman, and I. Strakovsky, eds., *Mini-Proceedings: Workshop on Physics with Neutral Kaon Beam at JLab* (K) (2016) arXiv:1604.02141 [hep-ph].
- [39] J. Hrtánková and A. Ramos, *Phys. Rev. C* **101**, 035204 (2020), arXiv:1910.01336 [nucl-th].
- [40] J. Öbertová, E. Friedman, and J. Mareš, *Phys. Rev. C* **106**, 065201 (2022), arXiv:2208.14946 [nucl-th].
- [41] A. Cieplý, J. Hrtánková, J. Mareš, E. Friedman, A. Gal, and A. Ramos, *AIP Conf. Proc.* **2249**, 030014 (2020), arXiv:2001.08621 [nucl-th].
- [42] A. Cieplý, M. Mai, U.-G. Meißner, and J. Smejkal, *Nucl. Phys. A* **954**, 17 (2016), arXiv:1603.02531 [hep-ph].
- [43] N. Wickramaarachchi, R. A. Schumacher, and G. Kalicy (GlueX), *EPJ Web Conf.* **271**, 07005 (2022), arXiv:2209.06230 [nucl-ex].
- [44] P. C. Bruns, A. Cieplý, and M. Mai, *Phys. Rev. D* **106**, 074017 (2022).
- [45] P. C. Bruns, (2024), arXiv:2408.08719 [nucl-th].
- [46] F. Sgaramella *et al.*, *Nuovo Cim. C* **47**, 285 (2024).
- [47] X.-L. Ren, E. Oset, L. Alvarez-Ruso, and M. J. Vicente Vacas, *Phys. Rev. C* **91**, 045201 (2015), arXiv:1501.04073 [hep-ph].
- [48] A. Feijoo, R. Molina, L. R. Dai, and E. Oset, *Eur. Phys. J. C* **82**, 1028 (2022), arXiv:2105.09654 [nucl-th].
- [49] J. Bulava *et al.* (Baryon Scattering (BaSc)), *Phys. Rev. D* **109**, 014511 (2024), arXiv:2307.13471 [hep-lat].
- [50] J. Bulava *et al.* (Baryon Scattering (BaSc)), *Phys. Rev. Lett.* **132**, 051901 (2024), arXiv:2307.10413 [hep-lat].
- [51] Z. Zhuang, R. Molina, J.-X. Lu, and L.-S. Geng, (2024), arXiv:2405.07686 [hep-ph].
- [52] X.-L. Ren, *Phys. Lett. B* **855**, 138802 (2024), arXiv:2404.02720 [hep-ph].
- [53] J. Nieves, A. Feijoo, M. Albaladejo, and M.-L. Du, *Prog. Part. Nucl. Phys.* **137**, 104118 (2024), arXiv:2402.12726 [hep-ph].
- [54] M. Conde-Correa, T. Aguilar, A. Capelo-Astudillo, A. Duenas-Vidal, J. Segovia, and P. G. Ortega, (2024), arXiv:2407.01759 [hep-ph].

- [55] K. Azizi, Y. Sarac, and H. Sundu, *Eur. Phys. J. C* **84**, 428 (2024), arXiv:2306.07393 [hep-ph].
- [56] V. M. Sarti, A. Feijoo, I. Vidaña, A. Ramos, F. Giacosa, T. Hyodo, and Y. Kamiya, *Phys. Rev. D* **110**, L011505 (2024), arXiv:2309.08756 [hep-ph].
- [57] S. Acharya et al. (ALICE), *Phys. Lett. B* **845**, 138145 (2023), arXiv:2305.19093 [nucl-ex].
- [58] A. Feijoo, M. Korwieser, and L. Fabbietti, (2024), arXiv:2407.01128 [hep-ph].
- [59] H.-P. Li, C.-W. Xiao, W.-H. Liang, J.-J. Wu, E. Wang, and E. Oset, (2024), arXiv:2409.05787 [hep-ph].
- [60] S. Acharya et al. (ALICE), *Eur. Phys. J. C* **83**, 340 (2023), arXiv:2205.15176 [nucl-ex].
- [61] S. Koonin, *Physics Letters B* **70**, 43 (1977).
- [62] S. Pratt, T. Csörgo, and J. Zimányi, *Physical Review C* **42**, 2646 (1990).
- [63] M. Albaladejo, A. Feijoo, J. Nieves, E. Oset, and I. Vidaña, (2024), arXiv:2410.08880 [hep-ph].
- [64] S. Acharya et al. (ALICE), *Phys. Lett. B* **811**, 135849 (2020), arXiv:2004.08018 [nucl-ex].
- [65] S. Acharya et al. (ALICE), (2023), arXiv:2311.14527 [hep-ph].
- [66] I. Vidaña, A. Feijoo, M. Albaladejo, J. Nieves, and E. Oset, *Physics Letters B* **996**, 138201 (2023).
- [67] A. Feijoo, D. Gazda, V. Magas, and A. Ramos, *Symmetry* **13**, 1434 (2021), arXiv:2107.10560 [hep-ph].
- [68] J. Torres-Rincón, A. Ramos, and L. Tolos, *Physical Review D* **108**, 096008 (2023).
- [69] S. Acharya et al. (ALICE), *Phys. Rev. Lett.* **124**, 092301 (2020), arXiv:1905.13470 [nucl-ex].
- [70] S. Acharya et al. (ALICE), *Phys. Lett. B* **833**, 137272 (2022), arXiv:2104.04427 [nucl-ex].
- [71] K. Miyahara, T. Hyodo, and W. Weise, *Phys. Rev. C* **98**, 025201 (2018), arXiv:1804.08269 [nucl-th].